Mononuclear and binuclear copper(II) bis(1,3-benzodioxole-5-carboxylate) adducts with bulky pyridines

Joan Soldevila-Sanmartín [a], José A. Ayllón [a,*], Teresa Calvet [b], Merce Font-Bardia [c], Josefina Pons [a,*]

a Departament de Química, Universitat Autònoma de Barcelona, 08193-Bellaterra, Barcelona, Spain

b Cristal·lografia, Mineralogia i Dipòsits Minerals, Universitat de Barcelona, Martí i Franquès s/n, 08028 Barcelona, Spain

c Unitat de Difracció de Raig-X, Centres Científics i Tecnològics de la Universitat de Barcelona (CCiTUB), Universitat de Barcelona, Solé i Sabarís, 1-3, 08028 Barcelona, Spain

E-mail addresses: JoseAntonio.Ayllon@uab.cat (J.A. Ayllón), Josefina.Pons@uab.cat (J. Pons).

32 **ABSTRACT:**

33

34 Copper(II) bis(1,3-benzodioxole-5-carboxylate) adducts with bulky pyridines have been prepared from

35 the reaction of copper(II) acetate with 1,3-benzodioxole-5-carboxylic acid (piperonylic acid, HPip) and

36 an excess of pyridine derivatives (3-phenylpyridine, 3-Phpy, 4-phenylpyridine, 4-Phpy, or 4-

37 benzylpyridine, 4-Bzpy). Using 3-Phpy or 4-Bzpy binuclear paddle wheel compounds ([Cu(l-Pip)2(3-

38 Phpy)]2 (1) and [Cu(l-Pip)2(4-Bzpy)]2 (3), and mononuclear complexes [Cu(l-Pip)2(3-Phpy)2(H2O)]

39 (2) and {[Cu(Pip)2(4-Bzpy)2]}{[Cu(Pip)2(4-Bzpy)2](HPip)} {4A}{4B} have been isolated.

40 Mononuclear 2 can also be produced from 1 in presence of an excess of 3-Phpy, while low thermal

41 treatment of 2 at 70 C, in absence of solvent, reverts to the formation of 1. On the other hand, 4

42 presents a singular structure that contains two independent mononuclear units {4A} and {4B}. Working

43 with 4-Phpy yields crystalline binuclear [Cu(l-Pip)(Pip)(4-Phpy)2]2 4CH3OH (5). In this complex only

44 half of the carboxylate ligands bridge copper atoms, being one of the rare examples of this flat core. Its

45 crystal structure contains a significant fraction of volume filled with methanol that is partly lost simply

46 by exposing the solid to air. However, this process is related to an irreversible structure collapse,

47 showing that the intermolecular interactions after methanol removal are not enough to support a porous

48 structure.

49

50

1. INTRODUCTION

The architecture of molecular coordination compounds is a key field of research, in special relative to its use as Secondary Building Units (SBUs) motifs to create supramolecular networks [1–4]. In this context, copper carboxylates have been extensively investigated due to the versatility of these ligands, which can adopt different coordination modes as illustrated in Fig. 1 [2,3]. The nature of the carboxylate ligand joint to the use of additional ligands determines the nuclearity and topological features of the formed compounds. Binuclear compounds formulated as [Cu (RCOO)2L]2 with a paddle-wheel topology are found in a vast amount of reports, with more than 1300 structures described [5]. The interest of the paddle-wheel motif is that both structural and functional changes can be achieved simply by varying the metal cores, the bridging moieties, or the axial ligands (L) [6]. This functional versatility makes them particularly attractive for the design and synthesis of many crystalline materials [7]. Other binuclear copper carboxylate complexes with different morphology are much less frequently reported [8–15]. Mononuclear complexes of type [Cu(RCOO)2L2] are also very usual. However, although the mononuclear-binuclear complex equilibria in solution has been reported in early studies [16], simultaneous isolation and structural characterization reports of monomer and dimer for a particular combination of carboxylate and auxiliary ligand are much more scarce [17,18].

We are interested in the study of 1,3-benzodioxole-5-carboxylate (piperonylic acid, HPip) copper complexes. The dioxole groups of this ligand would induce the formation of H-bond interaction network. Surprisingly, this carboxylate ligand has attracted little interest in the field of coordination chemistry, only few Zn(II) [19,20], Cd(II) [8,21–23], and Sn(II) [24] complexes have been reported. To the best of our knowledge, only one other Cu(II) compound containing this ligand has been reported recently by our group [25].

Continuing this work, here we introduce the use of substituted pyridines that can provide structural rigidity and thus determine the crystal packing. The different substituents can help to tune the subtle balance of energies, including both intramolecular and intermolecular bonds that determine molecular topology and supramolecular arrangement [26]. Since bulky pyridines including aromatic rings, such as 3-phenylpyridine (3-Phpy), 4-benzilpyridine (4-Bzpy) or 4-phenylpyridine (4-Phpy), show good affinity to copper(II) nucleus [27–30] we used them as auxiliary ligands to combine with the copper piperonylate.

In this work we report the crystal structures of five new compounds (1–5), characterize them via Elemental Analyses (EA), Infra-Red spectroscopy (IR), X-ray diffraction and discuss in deep their different topologies and supramolecular networks.

.

2. RESULTS AND DISCUSSION

2.1. Synthesis and general characterization

The reaction between $Cu(Ac)_2 \cdot H_2O$ with HPip and pyridine derivatives (dPy = 3-Phpy, 4-Bzpy, 4-Phpy) was essayed in MeOH using a 1:2:4 Cu:HPip:dPy molar ratio at room temperature and atmospheric pressure (Fig. 2). Pyridine derivatives were used in excess to neutralize the HAc byproduct. This strategy avoids the need of isolating the copper piperonylate, a compound which otherwise has not been reported. The corresponding crystals suitable for X-ray crystallographic analysis were grown via slow evaporation of the reaction mixture. Resulting complexes 1–5 were characterized via elemental analysis, IR spectra and X-ray diffraction. Based on the results herein reported, a differential behaviour between 3-Phpy and 4-Bzpy on one side and 4-Phpy in the other has been observed.

Using 3-Phpy as a ligand resulted in the isolation and characterization of two compounds (1 and 2) obtained sequentially from the same reaction mixture. Those compounds were a paddle-wheel binuclear and a mononuclear complex, respectively. When working with 4-Bzpy, once again two products (3 and 4) were isolated and characterized. Similarly to the results with 3-Phpy, a paddle wheel dimer (3) and a small amount of a mononuclear structure (4) were obtained. Compound 4, however, is fairly different from its counterpart 2, containing two crystallographic independent subunits (4A and 4B) in its unit cell. EA results are in agreement with the elucidated crystal structures. From now on, results obtained with 3-Phpy and 4-Bzpy are going to be analysed together due the similarity of their behavior when compared to 4-Phpy. For complexes 1–3, phase purity of the bulk samples was confirmed by X-ray powder diffraction (Figs. S1–S3).

In the case of 4-PhPy, a totally different result was obtained. Only one product was isolated (5). Although this product is binuclear, it shows notable differences respect to 1 and 3. Compound 5 has a 1:2:2 Cu:Pip:dPy ratio, which is the same found in mononuclear complexes. However, in this complex half of the carboxylate ligands are able to bridge the two metal centers, resulting in a nonpaddle wheel Cu(II) dimer. In fact, compounds with this core are rarely isolated. Compared to the more than 1300 paddle wheel Cu(II) dimers [5] reported in the literature, only eight [8–15] similar compounds have been reported. This topology allows for the accommodation of four MeOH molecules per dimer. Compound 5 is stable while immersed in the solvent, but loses MeOH when exposed to open atmosphere, according to EA and X-ray powder diffraction (XRPD).

ATR-FTIR spectra of the five compounds confirm the presence of organic ligands used in the synthesis including bands assignable to dPy and Pip anion (Figs. S4–S6). Bands assignable to carboxylate group give key information about the coordination mode [31]. Unsurprisingly, compounds 1 and 3 have a very similar IR spectrum. Thus, the difference between mas(COO) (1593 cm⁻1 for 1 and 1591 cm⁻1 for 3) and ms(COO) (1439 cm⁻1 for 1 and 1437 cm⁻1 for 3) is D = 154 cm⁻1, indicating bidentate bridging coordination mode of the carboxylates [31].

122 In 2, spectrum ν_{as}(COO) band can be identified at 1570 cm^{-1} and ν_s(COO) band at 1366 cm^{-1}. The

123 difference is Δ = 204 cm^{-1}, suggesting a monodentate coordination mode for the carboxylate ligands

124 [31]. Furthermore, a broad band can be seen at 3229 cm^{-1}, which is consistent with the presence of

125 H_2O in the structure. The shape and position of this band suggest that the – OH group participates in a

126 hydrogen bond interaction [32]. Spectrum of compound 4 includes bands that suggest the presence of

127 both protonated carboxylic acid (1674 cm^{-1}) and carboxylate anion (1597, 1566, 1501 and 1350

128 cm^{-1}). The presence of different bands attributable to ν_{as}(COO) and ν_s(COO) coordination modes is

129 consistent with the presence of both monodentate and bidentate carboxylate ligands [31], as confirmed

130 after structure elucidation.

131 Compound 5 also shows an intricate IR spectrum in the 1650–1300 cm^{-1} region, suggesting different

132 carboxylate coordination modes. In this spectrum we could also see a relatively broad band at 3421

133 cm^{-1}, which is consistent with the presence of absorbed MeOH in its structure.

134

135 2.2. Molecular and extended structure

136 2.2.1. Compounds containing 3-Phpy and 4-Bzpy

137 The reaction between Cu(Ac)2$\cdot$ H2O, HPip and 3-Phpy/4-Bzpy in MeOH yielded similar results. For

138 both, green crystals were isolated, resulting in paddle-wheel like dimers [Cu(l-Pip)2(3-Phpy)]2 (1) and

139 [Cu(l-Pip)2(4-Bzpy)]2 (3). From further evaporation of the mother liquors, mononuclear compounds

140 were isolated as blue monocrystals, with lower yield than the paddle-wheel like compounds. In the case

141 of 3-Phpy, monomer [Cu(Pip)2(3-Phpy)2(H2O)] (2) and, for 4-Bzpy, {[Cu(Pip)2(4-

142 Bzpy)2]$\cdot$ [Cu(Pip)2(4-Bzpy)2(-HPip)]} (4). Compound 4 has two monomers in its unit cell. As it can be

143 seen, the stoichiometry and topology of the mononuclear compounds differ much more from each other

144 than dimeric compounds obtained here. Therefore, dimeric compounds 1 and 3 will be described

145 together.

146 Binuclear compounds 1 and 3 (Fig. 3) were isolated as green prism-like crystals. Single crystal XRD

147 revealed that they are classical paddle wheel-like dimers. The ratio of Cu:Pip:dPy is 1:2:1, therefore, 1

148 and 3 contain four carboxylates in a syn-syn configuration bridging the two Cu(II) atoms. In those

149 centrosymmetric dimers Cu(II) ions adopt [CuO4N] coordination environment.

150 The four oxygens are provided by four different Pip ligands. The square pyramidal coordination

151 geometry (τ = 0) [33] is completed with an apical 3-Phpy (1) or 4-Bzpy (3) ligand coordinating through

152 the N atom. Cu–O distances, 1.960 Å–1.978 Å (1) and 1.967 Å–1.990 Å (3), and Cu–N distances, 2.175

153 Å (1) and 2.145 Å (3), are comparable to others found in the literature, as well as the Cu(II)$\cdots$ Cu(II)

154 separation within each carboxylate bridged dicopper(II) unit: 2.633 Å (1) and 2.652 Å (3) [34,35].

155 Selected distances and angles for 1 and 3 are provided in Table 1. Despite their similarities in angles and

156 interatomic distances, those compounds do not belong to the same symmetry group, one being P$\overline{1}$ (1)

157 and the other P21/c (3).

158   Both dimers are connected into compact 3D molecular arrangements through H-bond interactions,

159   dioxole rings of Pip ligand participating in many of the shorter ones. For 1, C25–H25B⬚ ⬚ ⬚ O2

160   involves a coordinated oxygen from a carboxylic group and a hydrogen provided by the dioxole ring,

161   while C11–H11⬚ ⬚ ⬚ O4 involves a hydrogen in ortho position of the 3-Phpy benzene ring and an

162   oxygen of the dioxole ring. Those interactions define 2D layer which stack one over another (Fig. 4, up).

163   For 3, the interactions are similar, involving the same groups. C6–H6B⬚ ⬚ ⬚ O5 contact links a

164   hydrogen from the dioxole ring and a coordinated oxygen from a carboxylic group, while C21–H21⬚ ⬚

165   ⬚ O7 interaction binds the hydrogen in para position of the pyridine ring and an oxygen of a dioxole

166   group. However, another kind of interaction, which does not appear in 1 occurs here, in the form of an

167   H⬚ ⬚ ⬚ p interaction, C22–H22A⬚ ⬚ ⬚ Cg1 (Cg1 = C10, C11, C12, C13, C15 and C16), which connects

168   the methylene group of 4-Bzpy and the aromatic ring of Pip ligand (Fig. 4, down). Other relevant

169   interatomic distances and angles for 1 and 3 are provided in Table 2.

170   Mononuclear compounds in the form of blue monocrystals were obtained as secondary products of the

171   formation reactions of paddle wheels 1 and 3. Contrary to 1 and 3, which have the same topology, 2 and

172   4 differ much more from each other. Compound 2 contains a single monomer, whereas compound 4

173   contains two crystallographic independent monomers, [Cu(Pip)2(4-Bzpy)2] (4A) and [Cu(Pip)2 (4-

174   Bzpy)2(HPip)] (4B) (see Fig. 2).

175   Compound 2 crystallizes in the monoclinic C2/c space group (Fig. 5). The Cu:Pip:dPy ratio is 1:2:2. The

176   Cu(II) atom has a [CuO3-N2] core in a slightly distorted square pyramidal geometry (s = 0.050) [33].

177   The basal plane is defined by two crystallographic equivalent oxygen atoms provided by two

178   monodentate Pip ligands (Cu1–O1 = 1.9351(12) Å) and a pair of nitrogen atoms provided by 3-Phpy

179   ligands (Cu1–N1 = 2.01(15) Å) both in trans positions. The apical position is occupied by a coordinated

180   H2O molecule (Cu1–O5 = 2.244(2) Å). Selected distances and angles are provided on Table 3.

181   Compound 2 shows a 1D supramolecular structure where H2O ligand plays a key role. Each H2O

182   molecule presents two symmetrical strong H-bond that connect its hydrogen atoms with the two non-

183   coordinating oxygens of the Pip ligand from an adjacent molecule, O5–H5O⬚ ⬚ ⬚ O2 1.844 Å, O5–

184   H5O 0.875 Å, H5O–O5⬚ ⬚ ⬚ O2 2.709 Å and O5–H5O⬚ ⬚ ⬚ O2 169.7⬚ (Fig. 6). This interaction

185   prevents the chelation of the Pip ligand. Furthermore, this interaction defines chains in the b direction

186   with intra-chain Cu(II)⬚ ⬚ ⬚ Cu(II) distances being 5.753 Å. It is interesting to see how the formation

187   of these chains also forces the two Pip ligands to point to the same direction, instead of having a more

188   common opposite facing. Similar 1D chains with a double H-bond are relatively scarce, with only a

189   reduced number (ca. 13) of other examples found in the literature [36–38].

190   In 4, each monomer contains a copper cation linked to two Pip ligands and two 4-Bzpy ligands (Fig. 7).

191   The main difference between the two monomers is due the presence of additional coordinating HPip

192   acid in molecule 4B. This HPip that presents a partial occupancy on the two apical positions, which

193   causes structural disorder, would led to hypothetical square pyramidal coordination geometry of Cu1B.

194   Furthermore, this solvating acid explains the differences in the coordination of anionic Pip ligands

between both molecules. Thus, while molecule 4A displays a distorted octahedral [CuO4N2] coordination environment, with oxygens provided by two clearly asymmetric, Cu1A–O1A, 1.983 Å and Cu1A–O2A, 2.488 Å, chelating Pip ligands, in molecule 4B, the presence of solvated HPip prevents the chelate coordination of Pip due steric factors. Consequently, molecule 4B shows a [CuO3N2] core and a square pyramidal geometry (s = 0) [33], distorted because the apical Cu1B–O2 vector has a 66.32⊡ angle with respect to the basal plane. The basal plane is formed by two oxygens provided by a Pip ligand acting as a monodentate ligand, Cu1B–O1B, 1.916 Å whereas Cu1B–O2B, 3.068 Å, is too long to be considered an effective interaction and nitrogen provided by two 4-Bzpy ligands in trans position, Cu1B-N1B, 2.003 Å. The coordination is completed with solvating HPip, by a relatively long Cu–O distance, Cu1B– O2, 2.567(3) Å, which could be attributed to the fact that the coordinating oxygen is protonated [39]. Table 4 lists selected bond distances and angles.

Both molecules 4A and 4B form independent 2D layers parallel to the ab plane. These layers stack in the c direction, in an AB pattern (Fig. 8). In 4A layers a double C–H⊡ ⊡ ⊡ O bridge between O2A atom from the carboxylate group with H12A (which belongs to the phenyl ring of the 4-Bzpy ligand) and H4A (which belongs to the pyridyl ring of the 4-Bzpy ligand) is responsible for the expansion of the supramolecular net in the a direction. In the b direction the layer is generated via interaction of H20B, linked to C20A atom of the dioxole ring and C1A, the ortho carbon of the pyridine ring of 4-Bzpy (Fig. 8). The 4B layer is held together via interactions of the monomeric units with the solvate HPip unit. Because of the disorder of the solvated HPip unit its structural role cannot be determined precisely. The two layers are linked through a C–H⊡ ⊡ ⊡ O bridge. It involves O4A from the Pip dioxole group of molecule 4A, which links with H9B of the phenyl ring of the 4-Bzpy ligand of molecule 4B. Distances and angles of relevant H-bonds are listed on Table 5.

2.2.2. Compounds containing 4-Phpy

Contrary to the previous results, only one compound is obtained when working with 4-Phpy (Fig. 9). This compound is a dimer, although it shows notable differences with compounds 1 and 3. First of all, the coordination of an extra dPy leads to the formation of a [CuO4N2] core for the centrosymmetric Cu(II) centers (compared to a [CuO4N] for 1 and 3). Furthermore, Pip ligands show a different behavior in 5. For 1 and 3 they act as syn-syn monodentate bridging dimers, whereas in 5 they act as an asymmetrically chelating ligand, Cu–O5 1.991 Å, Cu–O6 2.688 Å, and as a syn-anti bridging Pip ligand with distances such as Cu–O1 1.960 Å and Cu–O2 2.398 Å. This behavior is very rare, and only eight other compounds with this core have been reported. The octahedral coordination is completed via two nitrogen donors from 4-Phpy, Cu1–N1 2.003 Å and Cu1–N2 2.004 Å. The intradimer Cu⊡ ⊡ ⊡ Cu distance is 4.375(4) Å, compared to values of 2.633 Å–2.652 Å in 1 and 3. This distance is consistent with the fact that Cu⊡ ⊡ ⊡ Cu distances generally increase when decreasing the number of bridging carboxylate ligands [40]. Relevant distances and angles are provided in Table 6.

231   A comparison between intramolecular distances of 5 with other similar compounds found in the

232   literature can be seen in Table 7. This comparison reveals that all of them have a distorted octahedral

233   geometry, with apical oxygens being O6 of the chelate Pip and O2 from the bridging Pip. Otherwise, the

234   reported values of 5 are in the same range of those provided as references.

235   That octahedral coordination environment prevents the formation of a paddle-wheel dimer, resulting in

236   compound 5 having a rotor blade topology. The center of this dimer is a planar 8-membered ring

237   comprising Cu1–O1–C23–O2–Cu1–O1–C23–O2. The 4-Phpy ligands protrude almost perpendicularly

238   to that plane, resulting in a bulky and rigid structure. This structure is extended in a 3D network by

239   means of H-bonds (Table 8). Main forces in this network are interactions between C38-H38B ⬚ ⬚ C25

240   and C38–H38A ⬚ ⬚ O8, which correspond to adjacent Pip ligands (Fig. 10, up).

241   The rigid and bulky structure of the SBU leads to an inefficient packing. This causes the formation of

242   tridimensional elongated cavities (Fig. 10, down) that are only connected thought choke points defining

243   zig-zag channels. These channels occupy approxi mately 13% of the volume [41]. Those channels allow

244   the inclusion of MeOH, at a ratio of 4 MeOH molecules per Cu(II) dimer. The presence of absorbed

245   MeOH generates many additional H-bond interactions that contribute to formation of a 3D network.

246   Compound 5 has shown the loss of MeOH when exposed to open atmosphere and manipulated as

247   evidenced by EA, although it retains a crystalline structure. This fact led us to study the existence of

248   possible reversible absorption–desorption processes in 5. Some molecular materials, although not

249   intrinsically porous, are however permeable to volatile guests [42]. This means that the packed

250   molecules of the host are likely subjected to dynamic processes that allow small local reversible

251   structural rearrangements which create momentary voids where the guest molecules can be hosted or

252   diffuse [43]. In order to study the structural changes prompted by the entrapped solvent loss –

253   reabsorption when this complex is exposed to open atmosphere or methanol several XRD spectrums

254   were measured (Fig. 11). XRD patterns change show that the material suffers a structural

255   transformation. When the material is exposed to MeOH again, a new structural change occurs, but the

256   new XRD does not correspond to 5, denoting that 5 is only stable in contact with the mother liquor.

257

258   2.3. Interconversion between complexes 1 and 2

259   In this work, binuclear and mononuclear compounds containing 3-Phpy (1 and 2 respectively), were

260   isolated consecutively from the same reaction mixture. Studies of dimer-monomer interconversion are

261   scarcely found in the literature. We found that 2 can be obtained from 1 after dissolution in hot DMF

262   containing an excess of 3-Phpy (see experimental section). This process is reversible, after heating 2 at

263   70 ⬚ C for 24 h and crystalline 1 was obtained as confirmed by XRD, without the use of solvent. This

264   means that that half of the pyridine ligands show a labile character.

265

3. CONCLUSIONS

Direct reaction of copper acetate with piperonylic acid using and excess of pyridine derivative allowed the preparation of Cu (II) piperonylate-pyridine adducts. The room temperature reaction yields different mononuclear and binuclear compounds. This variability is favored by the ability of copper(II) to accommodate diverse coordination environments. The five described crystal structures evidenced that the coordination modes of this carboxylate ligand (Pip) in Cu(II) complexes could by modulated by addition of various pyridines. The combination of intermolecular interactions outlines different supramolecular networks. Dioxole ring of piperonylic acid has a key role in these interactions whereas p–p stacking interactions play a minor role. Two of the described crystal structures contain neutral molecules (solvating piperonylic acid in 4, methanol in 5) that after removal could a priori yield porous materials. However, collapsing of the crystal structure 5 after methanol removal denotes that the remaining interatomic con tacts have not enough strength to support the hypothetical resulting porous supramolecular framework.

4. EXPERIMENTAL SECTION

4.1. Materials and synthesis

Copper(II) acetate monohydrate (Cu(Ac)2 H2O), 1,3-benzodioxole-5-carboxylic acid (piperonylic acid, HPip), 3-phenylpyridine (3-Phpy), 4-benzylpyridine (4-Bzpy), 4-phenylpyridine (4-Phpy) and methanol (MeOH) were purchased from Sigma–Aldrich and used without further purification. All the reactions and manipulations were carried out in air.

4.1.1. [Cu(l-Pip)2(3-Phpy)]2. (1) and [Cu(Pip)2(3-Phpy)2(H2O)] (2)

To a solution of HPip (158.0 mg, 0.951 mmol) and 3-Phpy (354.0 mg, 2.281 mmol) in MeOH (20 mL) a green solution of Cu (Ac)2 H2O (98.0 mg, 0.492 mmol) in MeOH (20 mL) was added. The resulting light blue solution was allowed to evaporate at room temperature. When the solution volume was reduced to 15 mL, a green crystalline solid (1) appeared; it was filtered, washed twice with 5 mL of cold MeOH and dried under vacuum. Yield: 0.234 g (90%) (Respect to HPip).

After slow evaporation at room temperature, the mother liquor of the former synthesis yielded well-formed blue prism-like crystals (2). Compound 2, was filtered, washed twice with 2 mL of methanol and dried in the air. Yield: 0.041 g, (12%) (Respect to HPip). Compound 1: Elem. Anal. Calc. for C54H38N2O16Cu2 (1097.9): C, 59.07; H, 3.49; N, 2.55. Found C, 58.85; H, 3.47; N, 2.51%. ATR-FTIR (wavenumber, cm 1): 1633, 1594, 1500, 1488, 1439, 1387, 1258, 1240, 1194, 1171, 1111, 1078, 1031, 921, 875, 805, 772, 752, 722, 699, 683, 648. Compound 2: Elem. Anal. Calc. for C38H30N2O9Cu (722.2): C, 63.20; H, 4.19; N, 3.88. Found C, 63.02; H, 4.16; N, 3.93. ATR-FTIR (wavenumber, cm 1): 3230, 1570, 1500, 1476, 1439, 1366, 1257, 1236, 1211, 1135, 1110, 920, 895, 839, 813, 777, 752, 720, 696, 656.

4.1.2. [Cu(l-Pip)2(3-Phpy)]2. (1) to [Cu(Pip)2(3-Phpy)2(H2O)] (2) interconversion

78 mg (0.50 mmols) of 3-Phpy were added to a suspension of 116 mg of 2 (0.16 mmol) in DMF (20 mL). The mixture was heated until a homogenous solution was obtained, that was allowed to cool and partially evaporated at room temperature. A blue crystalline solid precipitated, which was filtered washed with methanol and dried in air. PXRD (Fig. S7) confirms the interconversion.

4.1.3. [Cu(l-Pip)2(4-Bzpy)]2. (3) and {[Cu(Pip)2(4-Bzpy)2]} {[Cu (Pip)2(4-Bzpy)2] (HPip)} (4)

To a solution of HPip (98.0 mg, 0.590 mmol) and 4-Bzpy (200.0 mg, 1.14 mmol) in MeOH (20 mL) a green solution of Cu (Ac)2 H2O (59.0 mg, 0.296 mmol) in MeOH (20 mL) was added. The resulting light blue solution was allowed to evaporate at room temperature. When the solution volume was reduced to 15 mL, a green crystalline solid appeared (3), it was filtered, washed twice with 5 mL of cold MeOH and dried under vacuum. Yield: 0.120 g (72%) (Respect to Cu(Ac)2 H2O).

317 After slow evaporation at room temperature, the mother liquor of the former synthesis yielded well-

318 formed blue-crystals (4). Compound 4 was filtered, washed twice with 2 mL of methanol and dried in

319 the air. Yield: 0.021 g, (9%) (Respect to Cu(Ac)2☐ H2O). Compound 3: Elem. Anal. Calc. for

320 C56H42N2O16Cu2 (1126.0): C, 59.73; H, 3.76; N, 2.49. Found C, 59.59; H, 3.91; N, 2.50%. ATR-

321 FTIR (wavenumber, cm☐ 1): 1633, 1591, 1503, 1437, 1384, 1255, 1239, 1170, 1111, 1074, 1033, 920,

322 885, 837, 804, 773, 721, 701, 682, 617.

323 Compound 4: Elem. Anal. Calc. for C88H70N4O20Cu2 (1630.6): C, 64.82; H, 4.33; N, 3.45. Found C,

324 65.11; H, 4.36; N, 3.39. ATR-FTIR (wavenumber, cm☐ 1): 2904, 1674, 1597, 1566, 1549, 1501, 1438,

325 1372, 1350, 1329, 1279, 1256, 1238, 1167, 1070, 1033, 923, 879, 858, 838, 806, 774, 734, 720, 684,

326 631, 615.

327

328 4.1.4. [Cu(l-Pip)(Pip)(4-Phpy)2]2☐ 4CH3OH (5)

329 To a solution containing HPip (120.0 mg, 0.722 mmol) and 4-Phpy (220.0 mg, 1.42 mmol) in MeOH

330 (20 mL), a green solution of Cu(Ac)2☐ H2O (69.0 mg, 0.346 mmol) in MeOH (20 mL) was added. A

331 turquoise blue solution was obtained and a small amount of powdered green precipitated was

332 immediately formed, that was filtered ad discarded. Then, after a few minutes a crystalline blue

333 precipitate was obtained. This precipitate was filtered and discarded. The remaining mother liquor was

334 concentrated almost to dryness. A blue crystalline solid appeared (5) that was filtered, washed twice

335 with 5 mL of cold MeOH and dried in the air. Yield: 0.130 g, (49%) (Respect to CuAc2☐ H2O).

336 Although the stoichiometry of compound 5 has been definitively stablished after resolution of their

337 crystal structure from single crystal XRD data, this compound losses solvent molecules after being

338 removed of the solution. For this reason, we found that the manipulation required to prepare the sample

339 for EA unavoidably leads to the loss of approximately half of the initial MeOH amount and thus result

340 were adjusted considering a [Cu(l-Pip)(Pip)(4-Phpy)2]2☐ 2CH3OH stoichiometry. % Calc. for

341 C78H64N4O18Cu2 (1472.5): C, 63.63; H, 4.38; N, 3.81. Found C, 63.54; H, 4.13; N, 3.82. ATR-FTIR

342 (wavenumber, cm☐ 1): 3420, 2907, 1614, 1555, 1502, 1484, 1434, 1349, 1251, 1166, 1074, 1032,

343 921,840, 804, 765, 736, 721, 696, 626.

344

345 4.2. Characterization

346 Elemental analyses (C, H, N) were carried out on a Euro Vector 3100 instrument. IR spectra were

347 recorded at the on a Tensor 27 (Bruker) spectrometer, equipped with an attenuated total reflectance

348 (ATR) accessory model MKII Golden Gate with diamond window in the range 4000–600 cm☐ 1. XRPD

349 patterns were measured with Siemens D5000 apparatus using the CuKa radiation. Patterns were

350 recorded from 2h = 5 to 50☐ , with a step scan of 0.02☐ counting for 1 s. at each step.

351 The X-ray intensity data for the crystallographic analysis of monocrystals were measured on a D8

352 Venture system equipped with a multilayer mono-chromate and a Mo microfocus (k = 0.71073 Å).

353 Frames were integrated with the Bruker SAINT Software package using a narrow-frame algorithm. The

354   structures were solved using the Bruker SHELXTL Software, package and refined using SHELX [44].

355   For 1–5, the final cell constants and volume, are based upon the refinement of the XYZ-centroids of

356   reflections above 20 r(I). Data were corrected for absorption effects using the multi-scan method

357   (SADABS). Crystal data and additional details of structure refinement for compounds 1–5, are included

358   in the supporting information. Figures were generated using Mercury software [45,46].

359

360 **ACKNOWLEDGEMENTS**

361

365

REFERENCES

[1] E. Coropceanu, A. Rija, V. Lozan, I. Bulhac, G. Duca, V.Ch. Kravtsov, P. Bourosh, Cryst. Growth Des. 16 (2016) 814.

[2] J. Thomas-Gipson, G. Beobide, O. Castillo, M. Fröba, F. Hoffmann, A. Luque, S. Pérez-Yañez, P. Román, Cryst. Growth Des. 14 (2014) 4019.

[3] J. Thomas-Gipson, R. Pérez-Aguirre, G. Beobide, O. Castillo, A. Luque, A. Pérez-Yañez, P. Román, Cryst. Growth Des. 15 (2015) 975.

[4] A.M. Beatty, Coord. Chem. Rev. 246 (2003) 131.

[5] Cambridge Structural Database (CSD) (Version 5.37, May 2016).

[6] M. Köberl, M. Cokoja, W.A. Herrmann, F.E. Kühn, Dalton Trans. 40 (2011) 6834.

[7] V. Paredes-García, R.C. Santana, R. Madrid, A. Vega, E. Spodine, D. Venegas-Yazigi, Inorg. Chem. 52 (2013) 8369.

[8] P. Segl'a, M. Palicová, D. Miklos, M. Koman, M. Melník, M. Korabik, J. Morzinski, T. Glowiak, M.R. Sundberg, P. Lönnecke, Z. Anorg. Allg. Chem. 630 (2004) 470.

[9] J. Moncol, M. Mudra, P. Lönnecke, M. Hewitt, M. Valko, H. Morris, J. Svorec, M. Melnik, M. Mazur, M. Koman, Inorg. Chim. Acta 360 (2007) 3213.

[10] M. Perec, R. Baggio, Acta Cryst. Sect. E Struct. Rep. Online 66 (2010) m275.

[11] E. Yang, W. Feng, J. Wang, X. Zhao, Inorg. Chim. Acta 363 (2010) 308.

[12] M. Sertcelik, N. Caylak Delibas, N. Necefoglu, T. Hokelek, Acta Cryst. Sect. E. Struct. Rep. Online 69 (2013) m290.

[13] J.A. Kitchen, P.N. Martinho, G.G. Morgan, T. Gunnlaugsson, Dalton Trans. 43 (2014) 6468.

[14] H. Wang, V. Safarifard, S.-Y. Wang, L.-H. Tu, H.-P. Xiao, B.-F. Huang, X.-H. Li, M. Payehghadr, A. Morsali, RSC Adv. 4 (2014) 11423.

[15] M. Fontanet, M. Rodríguez, X. Fontrodona, I. Romero, C. Viñas, F. Teixidor, Dalton Trans. 44 (2015) 10399.

[16] P. Sharrock, M. Melnik, Can. J. Chem. 63 (1985) 52.

[17] I.Y. Ahmed, A.L. Abu Hijlejh, Inorg. Chim. Acta 61 (1984) 241.

[18] B. Kozlevcar, A. Murn, N. PodlipnikK, N. Lah, I. Leban, P. Segedin, Croat. Chem. Acta 77 (2004) 613.

[19] S. Jin, Y.-T. LuO, D. Wang, J. Shi, S.W. Li, S.H. Shen, Y.J. Xu, Z. Anorg, Allg. Chem. 640 (2014) 1717.

[20] S. Jin, D. Wang, Z. Anorg, Allg. Chem. 637 (2011) 618.

[21] S. Jin, H. Liu, G. Chen, Z. An, Y. Lou, K. Huang, D. Wang, Polyhedron 95 (2015) 91.

[22] S. Jin, Y. Huang, D. Wang, H. Fang, T. Wang, P. Fu, L. Ding, Polyhedron 60 (2013) 10.

[23] S. Jin, H. Zhang, K. Xu, X. Ye, Y. Zhang, Y. Fang, D. Wang, Polyhedron 95 (2015) 108.

402 [24] M. Hanif, M. Hussain, S. Ali, M.H. Bhatti, M.S. Ahmed, B. Mizra, H.S. Evans, Turk. J. Chem.
403 31 (2007) 349.

404 [25] J. Soldevila-Sanmartín, J.A. Ayllón, T. Calvet, M. Font-Bardia, J. Pons, Inorg. Chem. Commun.
405 71 (2016) 90.

406 [26] M.-Y. Zhang, Z. Wang, T. Yang, Y. Zhang, X.-F. Ma, Z.-W. Ouyang, M. Kurmoo, M.-H. Zeng,
407 Chem. Eur. J. 22 (2016) 13900.

408 [27] D.V. Soldatov, G.D. Enright, J.A. Ripmeester, Chem. Mater. 14 (2002) 348.

409 [28] L. Loots, J.P. O'Connor, T. le Roex, D.A. Haynes, Cryst. Growth Des. 15 (2015) 5849.

410 [29] C.H. Springsteen, R.D. Sweeder, R.L. LaDuca, Cryst. Growth Des. 6 (2006) 2308.

411 [30] C.H. Springsteen, L.L. Johnston, R.L. LaDuca, Solid State Sci. 9 (2007) 804.

412 [31] K. Nakamoto, Infrared and Raman spectra of inorganic and coordination compounds, in:
413 Applications in Coordination, Organometallic and Bioinorganic Chemistry, sixth ed., Wiley-
414 Interscience, New York, USA, 2009.

415 [32]   J.A. Pérez, V. Montoya, J.A. Ayllón, M. Font-Bardia, T. Calvet, J. Pons, Inorg. Chim. Acta 394
416 (2013) 21.

417 [33] A.W. Addison, T.N. Rao, J. Chem. Soc., Dalton Trans. 7 (1984) 1349.

418 [34] K. Hassanein, O. Castillo, C.J. Gómez-García, F. Zamora, P. Amo-Ochoa, Cryst
419 Growth Des. 15 (2015) 5485.

420 [35] M. Tas, A. Titiz, E. Karabag, M. Kaya, M. Ataseven, H. Dal, Synth. React. Inorg. Met. Org.
421 Chem. 43 (2013) 1212.

422 [36] F. Hamza, G. Kickelbick, Macromolecules 42 (2009) 7762.

423 [37] Z. Vasková, N. Kitanovski, Z. Jaglicic, P. Strauch, Z. Ruzickováf, D. Valigur, M. Koman, B.
424 Kozlevcar, J. Moncol, Polyhedron 81 (2014) 555.

425 [38] N. Bozkurt, T. Tunç, N.Ç. Delibas, H. Necefoglu, T. Hökelek, Acta Cryst. E69 (2013) m458.

426 [39] V.M. Rao, D.N. Sathyanarayana, H. Manohar, J. Chem. Soc., Dalton Trans. (1983) 2167.

427 [40] G. Psomas, C.P. Raptopolou, L. Iordanidis, C. Dendrinou-Samara, V. Tangoulis, D.P.
428 Kessissoglou, Inorg. Chem. 39 (2000) 3042.

429 [41] A.L. Speck, J. Appl. Crystallogr. 36 (2003) 7.

430 [42] L.J. Barbour, Chem. Commun. (2006) 1163.

431 [43] A. Bacchi, P. Pelagatti, CrystEngComm 18 (2016) 6114.

432 [44] G.M. Sheldrick, Acta Cryst. C71 (2015) 3.

433 [45] C.F. Macrae, P.R. Edgington, P. McCabe, E. Pidcock, G.P. Shields, R. Taylor, M. Towler, J.
434 van de Streek, J. Appl. Crystallogr. 39 (2006) 453.

435 [46] C.F. Macrae, I.J. Bruno, J.A. Chisholm, P.R. Edgington, P. McCabe, E. Pidcock, L. Rodriguez-
436 Monge, R. Taylor, J. van de Streek, P.A. Wood, J. Appl. Crystallogr. 41 (2008) 466.

437

Legends to figures

Figure. 1 Coordination modes of carboxylate ligands.

Figure. 2 Scheme of the reactions carried out in this work. Isolated and characterized products are shown with their numbering scheme. Compound's 4B solvating HPip has been removed for the sake of clarity.

Figure. 3 [Cu(Pip)2(3-Phpy)]2 (1, left) and [Cu(Pip)2(4-Bzp)]2 (3, right), showing all non-hydrogen atoms and the atom numbering scheme; 50% probability amplitude displacement ellipsoids are shown.

Figure. 4 3D supramolecular network formed by the propagation of the hydrogen bond (blue line) of compounds 1 (up) and 3 (down). Hydrogens not participating in intermolecular contacts were omitted for clarity (Colour online).

Figure 5. [Cu(Pip)2(3-Phpy)2(H2O) (2), showing all non-hydrogen atoms and the atom numbering scheme; 50% probability amplitude displacement ellipsoids are shown.

Figure 6 3D supramolecular network for 2 (right) and detail of the 1D H-bonded (blue line) chains (left) (Colour online).

Figure 7 Molecule 4A (up) and 4B (down), showing all non-hydrogen atoms and the atom numbering scheme; 50% probability amplitude displacement ellipsoids are shown. For compound 4B the solvated HPip molecule is not shown for the sake of clarity.

Figure 8 Supramolecular structure of compound 4. Solvating HPip and hydrogens atoms omitted for clarity (up). Layer generated by the propagation of intermolecular contacts between A molecules in compound 4 (down).

Figure 9 [Cu(Pip)2(4-Phpy)2]2⎕ 4(MeOH) (5) showing all non-hydrogen atoms and the atom numbering scheme; 50% probability amplitude displacements are shown.

Figure 10 Transversal cut of the 2D network generated by propagating intermolecular contacts in compound 5 (left), cavities generated after hypothetical MeOH removing in compound 5 (right)..

Figure 11 Calculated pattern from resolved crystal structure of 5, from monocrystal XRD measured at 100 K (down). X-ray powder diffractogram of sample obtained after drying 5 in ambient, corresponding

475 to a [Cu(Pip)2(4-Phpy)2]2⬚ 2(MeOH) stoichiometry according to elemental analyses (middle). X-ray

476 powder diffractogram of the former sample after being exposed to clean MeOH and dried again at room

477 temperature (up).
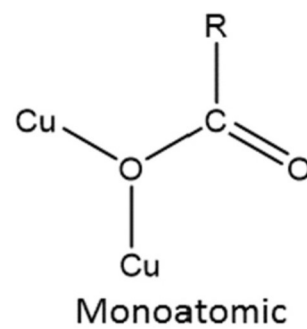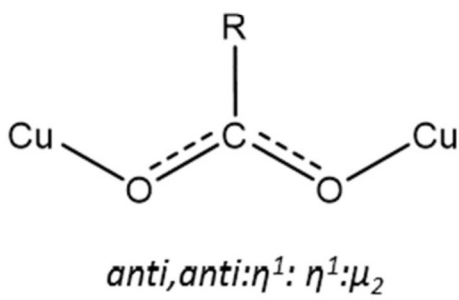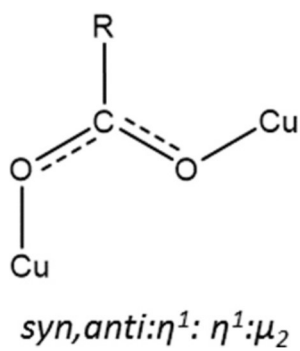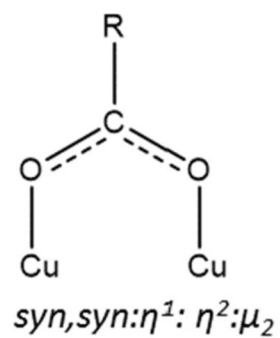
478

479

480

481

482

483

484

485
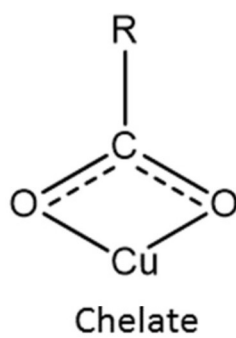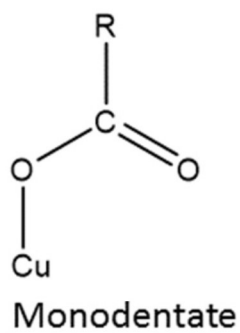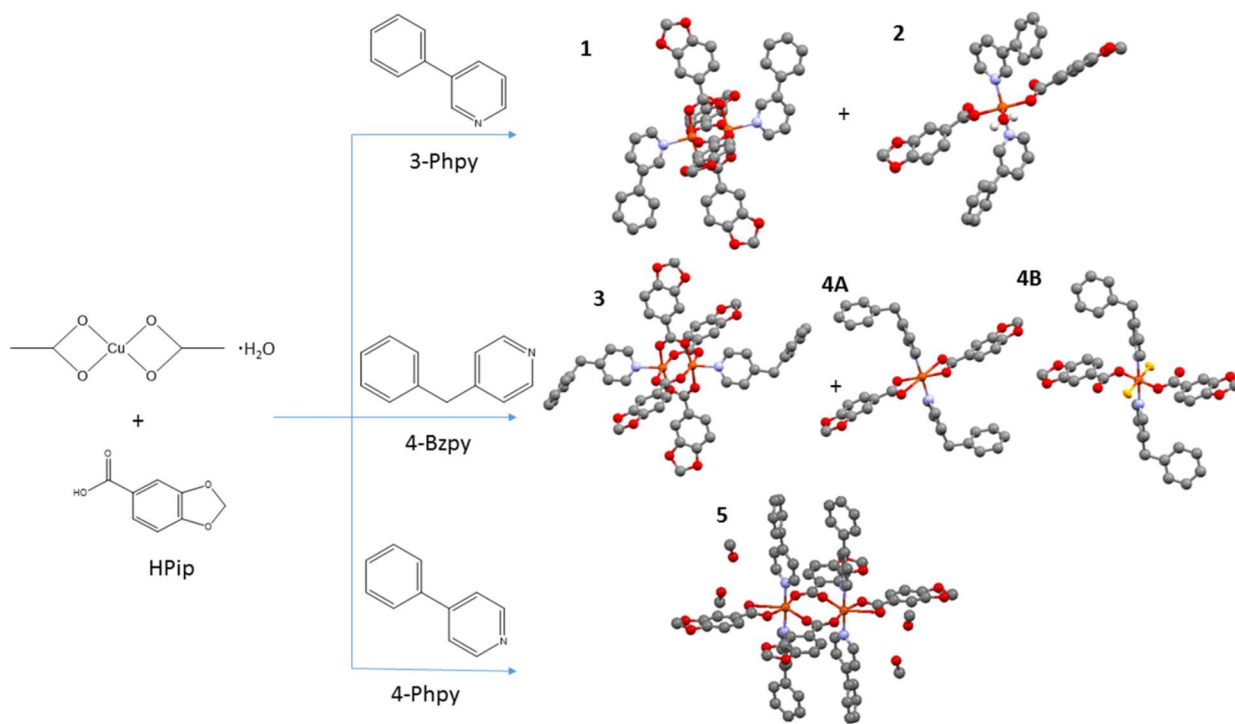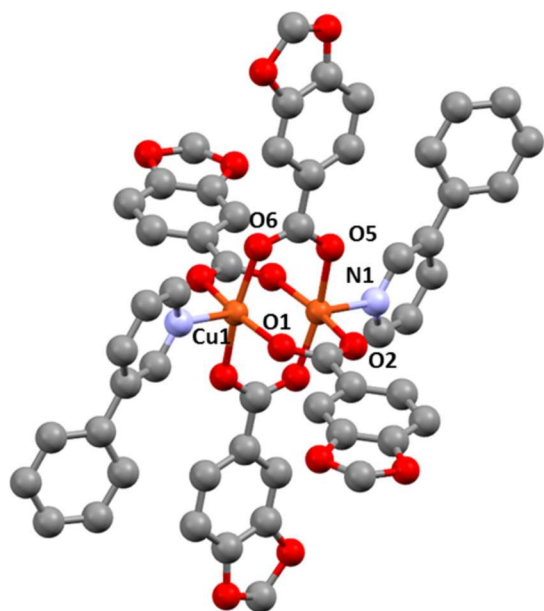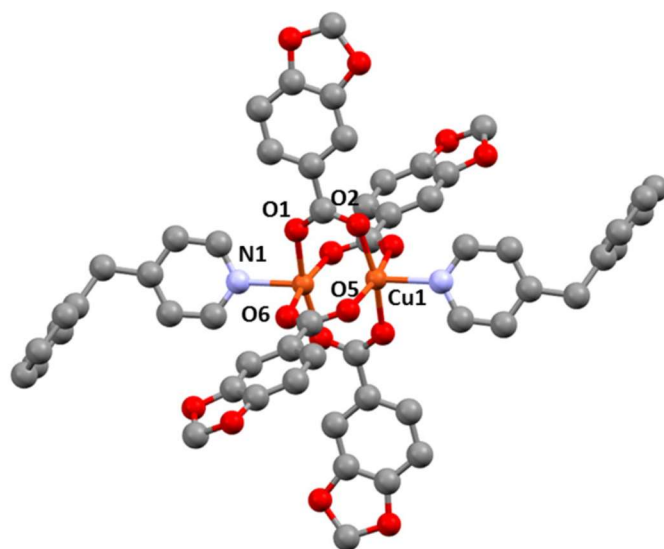
FIGURE 1

Monodentate

Chelate

$syn,syn:\eta^1: \eta^2:\mu_2$

$syn,anti:\eta^1: \eta^1:\mu_2$

$anti,anti:\eta^1: \eta^1:\mu_2$

Monoatomic

FIGURE 2

496

497

1   **3**

498

499

FIGURE 4

FIGURE 5

FIGURE 6

FIGURE 7

4A

4B
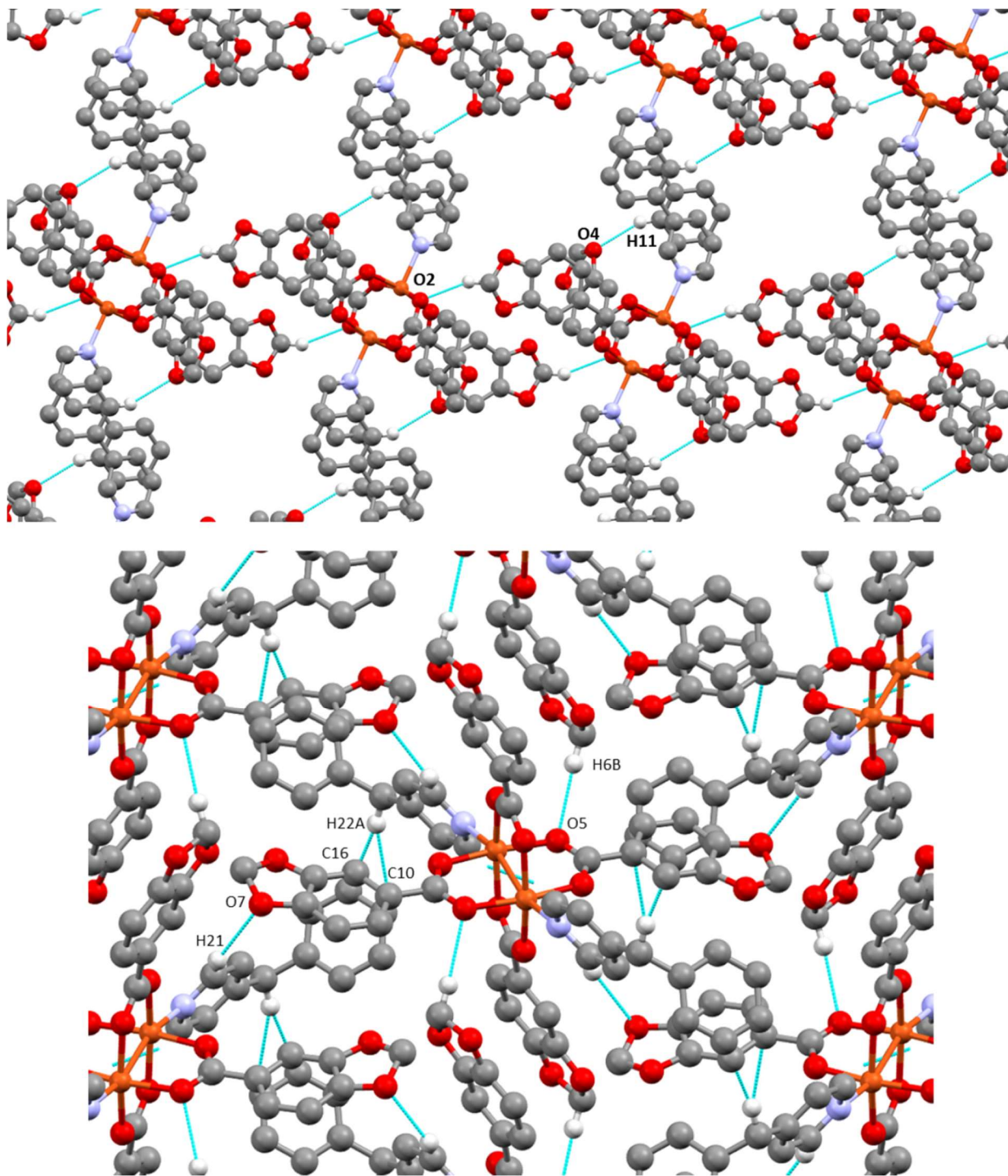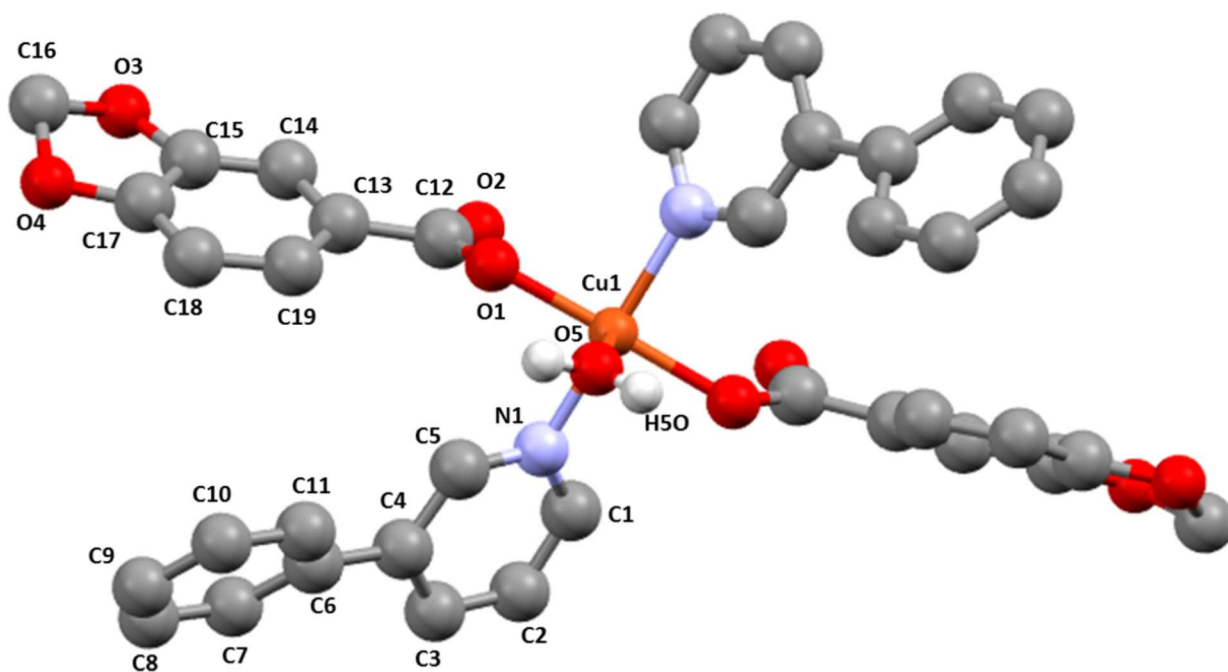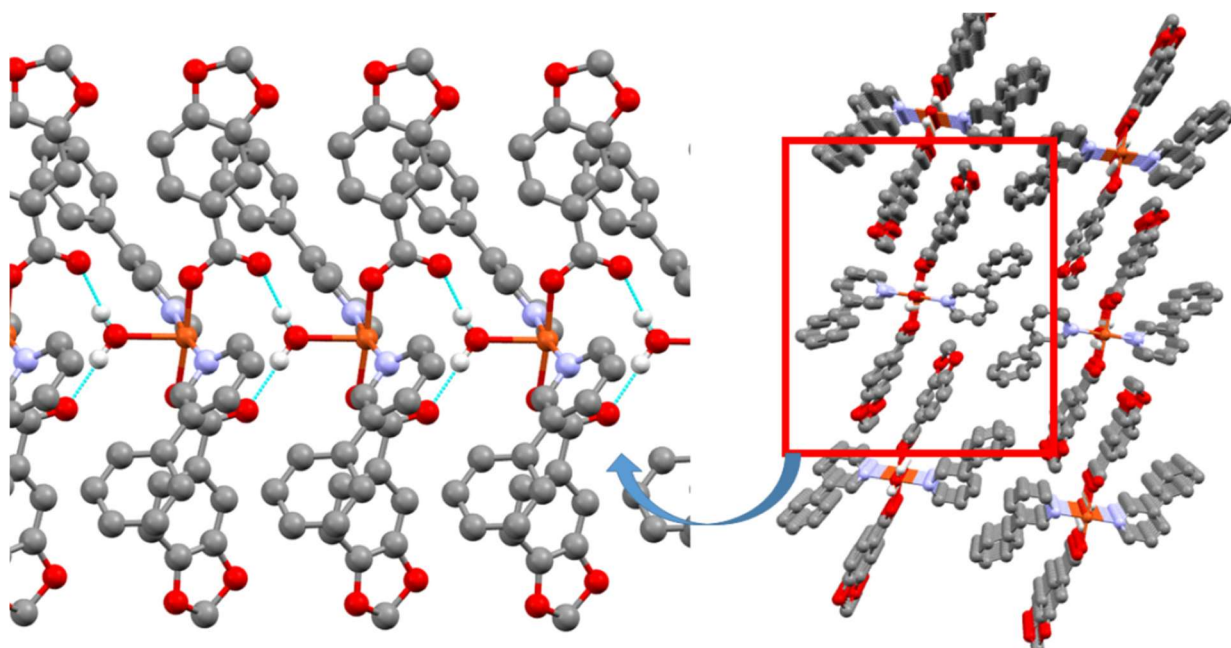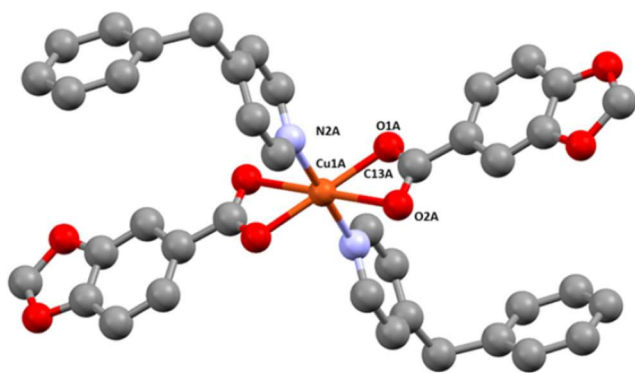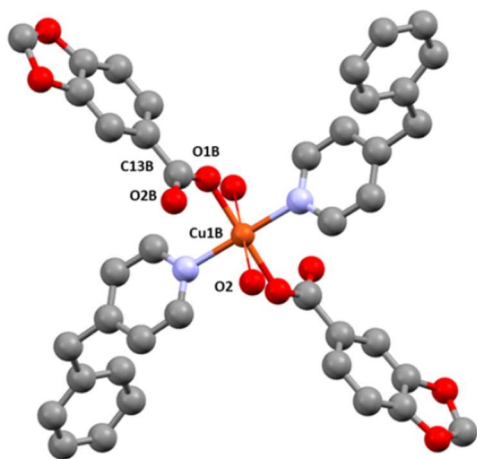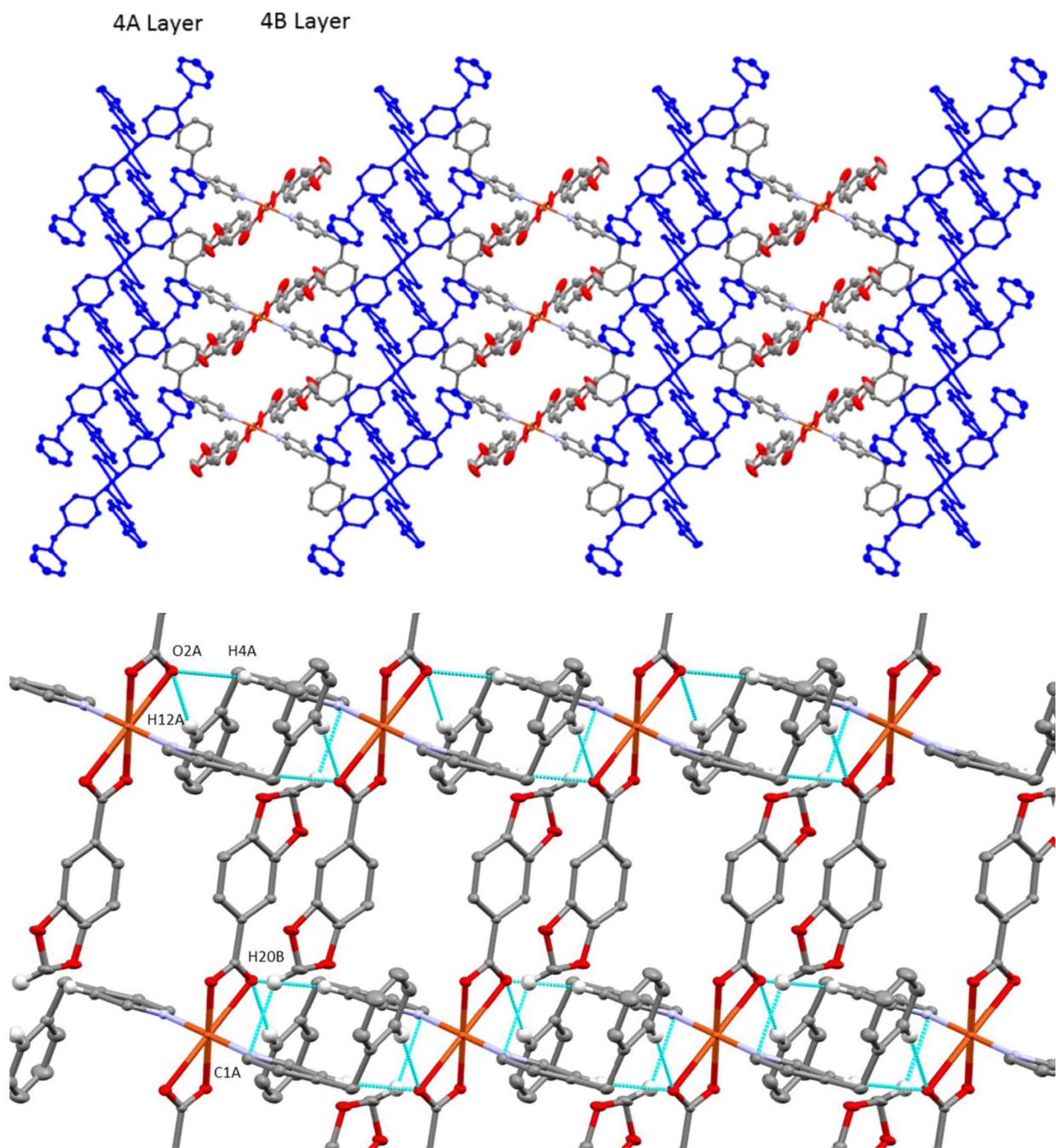
FIGURE 8

525
526   **FIGURE 9**

527

528
529
530
531
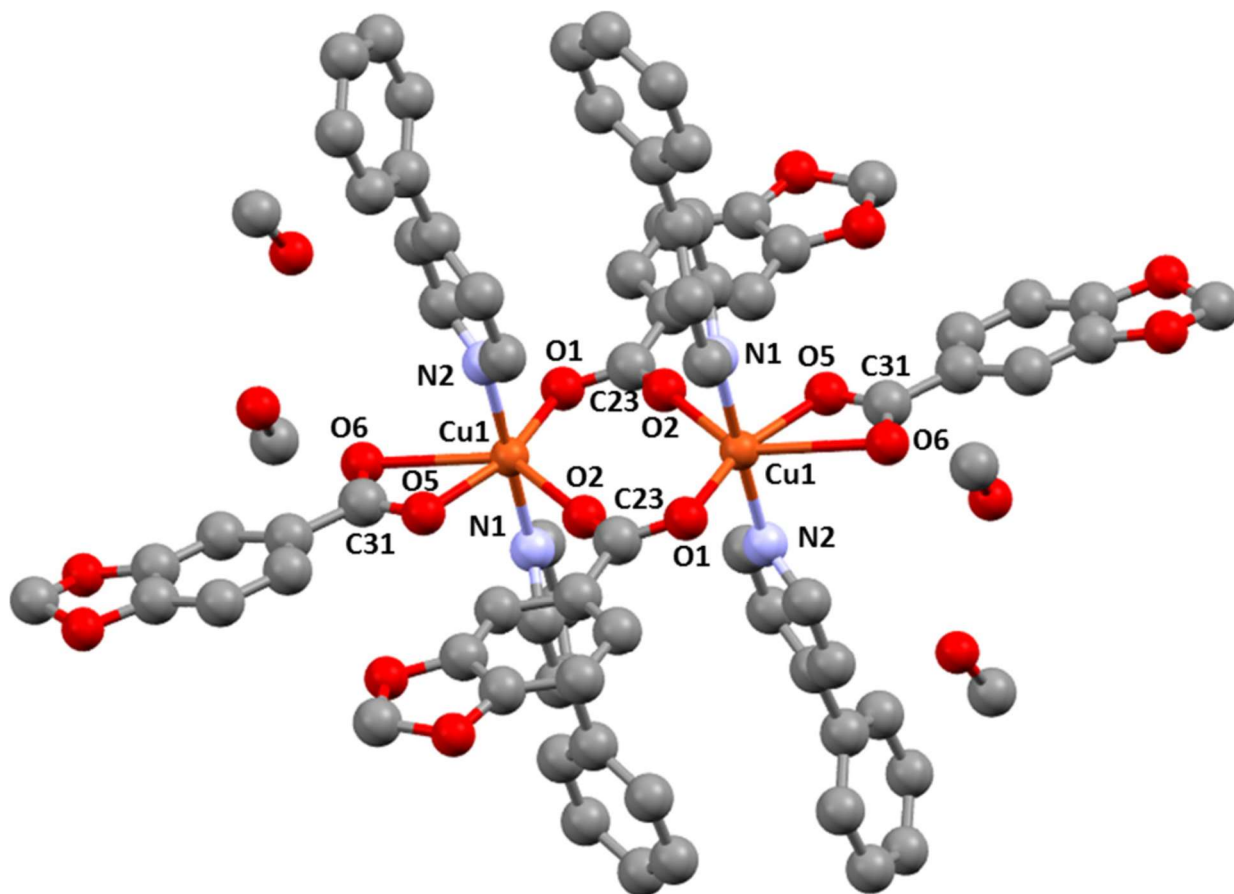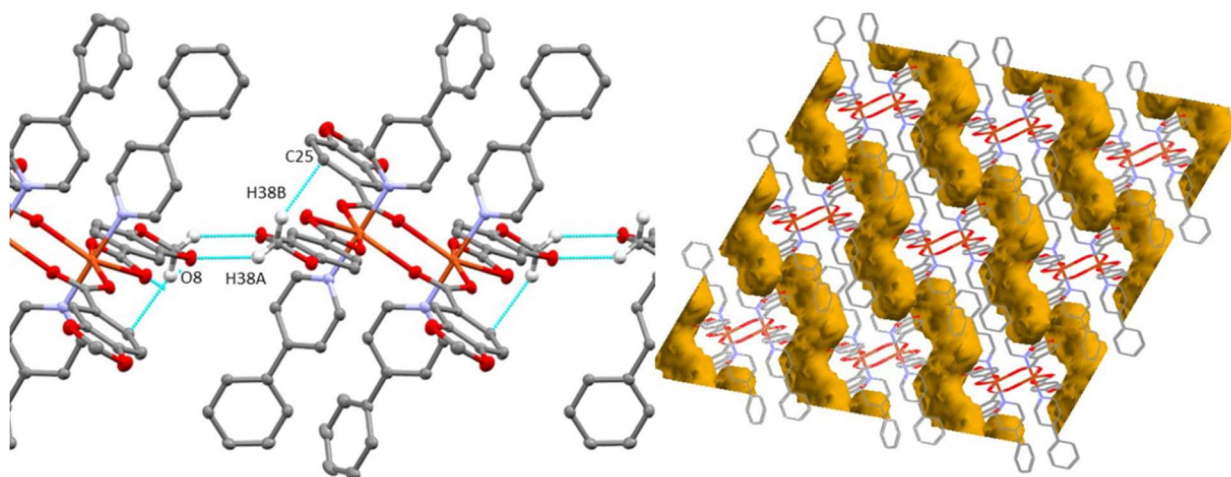
FIGURE 10
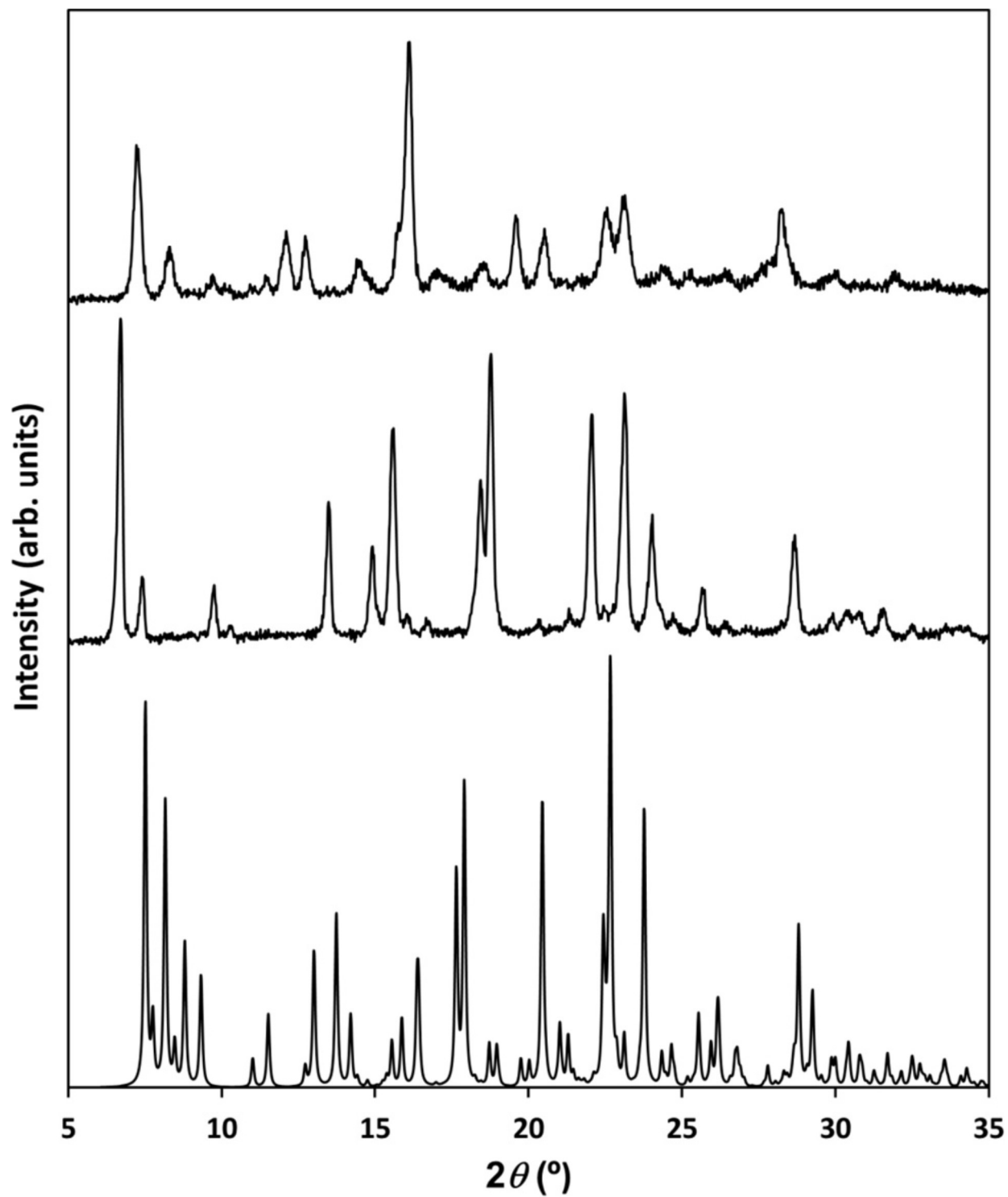
FIGURE 11

542 **Table 1** Selected bond lengths (Å) and angles (□) for 1 and 3. The estimated standard deviations

543 (e.s.d.s.) are shown in parentheses.

544

1		**3**	
Distances			
Cu1–O1	1.978(2)	Cu1–O1	1.967(2)
Cu1–O2	1.979(2)	Cu1–O2	1.990(2)
Cu1–O5	1.960(2)	Cu1–O5	1.978(2)
Cu1–O6	1.960(2)	Cu1–O6	1.973(2)
Cu1–N1	2.175(2)	Cu1–N1	2.145(3)
Cu1···Cu1	2.6331(6)	Cu1···Cu1	2.6518(8)
Angles			
O1–Cu1–O2	168.38(2)	O1–Cu1–O2	168.22(11)
O1–Cu1–O5	88.70(9)	O1–Cu1–O5	90.30(10)
O1–Cu1–O6	91.15(9)	O1–Cu1–O6	87.11(11)
O2–Cu1–O5	88.93(9)	O2–Cu1–O5	89.18(10)
O2–Cu1–O6	88.91(8)	O2–Cu1–O6	90.94(11)
O6–Cu1–O5	168.44(8)	O6–Cu1–O5	167.81(10)
O1–Cu1–N1	86.17(18)	O1–Cu1–N1	100.76(11)
O6–Cu1–N1	95.12(1)	O6–Cu1–N1	91.32(10)
O5–Cu1–N1	96.41(8)	O5–Cu1–N1	100.87(10)
O2–Cu1–N1	105.40(8)	O2–Cu1–N1	90.89(11)

545

546

547   **Table 2** Hydrogen bonding distances (Å, ⁰) for 1 and 3.

548

	D–H···A	D–H	H–D···A	D–H···A
1				
C25–H25B···O2	2.482	0.990	3.259	135.13
C11–H11···O4	2.498	0.950	3.319	144.79
C23–H23···O2	2.591	0.951	3.437	148.26
3				
C6–H6B···O5	2.515	0.971	3.450	161.63
C22–H22A···Cg1	2.759	0.970	3.722	172.17
C21–H21···O7	2.564	0.930	3.384	147.20
C27–H27···O4	2.647	0.930	3.473	148.29

549

550

551   **Table 3** Selected bond lengths (Å) and angles (⃞) for 2. The estimated standard deviations (e.s. d.s.) are

552   shown in parentheses.

553

Distances			
Cu1–O1	1.9351(12)	Cu1···O2	3.147
Cu1–N1	2.0096(15)	Cu1–O5	2.224(2)
Angles			
O1–Cu1–O1#1	176.02(9)	O1–Cu1–N1	91.74(6)
O1#1–Cu1–N1	88.51(6)	N1–Cu1–N1#1	172.82(10)
O1–Cu1–O5	88.01(4)	N1–Cu1–O5	93.59(5)

554

555

556 **Table 4** Selected bond lengths (Å) and angles (□) of 4. The estimated standard deviations (e.s.d. s.) are

557 shown in parentheses.

558

Molecule 4A			
Cu1A–O1A	1.9829(11)	O1A–Cu1A–O1A#1	180.0
Cu1A–O2A	2.488(1)	O1A–Cu1A–N2A	90.84(5)
Cu1A–N2A	2.0018(13)	O2A–Cu1A–O2A#1	180.0
		O2A–Cu1A–N2A	92.41
		O1A–C1A–O2A	122.39
Molecule 4B			
Cu1B–O1B	1.9158(16)	O1B–Cu1B–O1B	180.0
Cu1B–N1B	2.0036(15)	O2B–Cu1B–N1B	91.07(7)
Cu1B···O2B	3.068(1)	N1B–Cu1B–N1B	180.0(10)
		O1B–C13B–O2B	126.02

559

560

561

562 **Table 5** Hydrogen bond distances (Å, ⁰) of 4.

563

4A	C–H···O	C–H	C–H···O	C–H···O
C12A–H12A···O2A	2.553	0.951	3.431	153.71
C4A–H4A···O2A	2.431	0.950	3.3228	157.34
C20A–H20B··C1A	2.703	0.990	3.465	134.05
4A–4B				
C9B–H9B···O4A	2.551	0.951	3.224	127.90
C6B–H6BA···C19A	2.686	0.991	3.554	146.48

564

565

566 **Table 6** Selected bond lengths (Å) and angles (∣) of 5. The estimated standard deviations (e.s.d.s.) are

567 shown in parentheses.

568

5			
Distances			
Cu1–O1	1.9605(15)	Cu1–N2	2.0044(17)
Cu1–O5	1.9910(14)	Cu1–O2	2.3979(15)
Cu1–N1	2.0032(17)	Cu1···O6	2.688
Cu1···Cu1	4.375		
Angles			
O1–Cu1–O5	159.14(6)	N1–Cu1–N2	178.34(7)
O1–Cu1–N1	91.02(7)	O1–Cu1–O2	118.02(6)
O5–Cu1–N1	90.60(6)	O5–Cu1–O2	82.83(5)
O1–Cu1–N2	88.47(7)	N1–Cu1–O2	87.38(6)
O5–Cu1–N2	89.31(6)	N2–Cu1–O2	94.26(6)

569

570

571 **Table 7** Selected bond lengths (Å) of 5 and of previously reported compounds containing a similar core

572

	Carboxylate coordination mode	Cu⋯Cu	Cu–O (chelate, long)	Cu–O (chelate, short)	Cu–O (bridging, short)	Cu–O (bridging, long)	Cu–N2	Cu–N1
[8]	syn-anti	4.454	2.723	1.966	1.933	2.384	1.978	1.966
[9]	syn-anti	3.946	2.555	2.098	1.990	2.230	2.012	2.015
[10]	syn-anti	4.061	2.742	2.020	1.952	2.271	2.047	2.027
[11]	syn-anti	4.283	1.980	2.786	1.970	2.330	1.996	1.986
[12]	syn-anti	4.155	1.994	2.736	1.949	2.242	2.033	2.013
[13]	syn-anti	4.478	1.963	2.657	1.931	2.282	2.023	2.022
[14]	syn-anti	4.232	2.753	2.012	1.982	2.326	1.987	1.976
[15]	Syn-anti	4.438/ 4.577	2.739/2.740	1.992/1.9991	1.962/1966	2.383/2.353	2.011/ 2.024	2.009/ 2.016
5	**syn-anti**	**4.375**	**2.688**	**1.991**	**1.961**	**2.398**	**2.004**	**2.003**

573

574

575 **Table 8** Hydrogen Bonding distances (Å, ⏿) for compound 5.

576

	C–H···O	C–H	C–H···O	C–H···O
C38–H38A···O8	2.432	0.990	3.255	140.11
C20–H20···O7	2.707	0.950	3.631	164.43
C16–H16···O7	2.681	0.949	3.310	124.24
C9–H9···O4	2.683	0.950	3.391	131.86
C8–H8···O3	2.616	0.951	3.376	137.21
C18–H18···O2W	2.503	0.949	3.234	133.89
C33–H33···O1W	2.527	0.950	3.391	151.48

577